Immunity
Article

Redox Regulation of Interleukin-4 Signaling

Pankaj Sharma,[1,6] Rikhia Chakraborty,[1,2,6] Lu Wang,[3] Booki Min,[3] Michel L. Tremblay,[4] Tsukasa Kawahara,[5] J. David Lambeth,[5] and S. Jaharul Haque[1,*]
[1]Department of Cancer Biology, Lerner Research Institute, Cleveland Clinic, Cleveland, OH 44195, USA
[2]Department of Biological, Geological, and Environmental Sciences, Cleveland State University, Cleveland, OH 44115, USA
[3]Department of Immunology, Lerner Research Institute, Cleveland Clinic, Cleveland, OH 44195, USA
[4]McGill Cancer Centre, McGill University, Montreal, Quebec H3G 1Y6, Canada
[5]Department of Pathology and Laboratory Medicine, Emory University Medical School, Atlanta, GA 30322, USA
[6]These authors contributed equally to this work
*Correspondence: haquej@ccf.org
DOI 10.1016/j.immuni.2008.07.019

SUMMARY

The physiologic control of cytokine receptor activation is primarily mediated by reciprocal activation of receptor-associated protein tyrosine kinases and protein tyrosine phosphatases (PTPs). Here, we show that immediately after ligand-dependent activation, interleukin (IL)-4 receptor generated reactive oxygen species (ROS) via phosphatidylinositol 3-kinase-dependent activation of NAD(P)H oxidase (NOX)1 and NOX5L. ROS, in turn, promoted IL-4 receptor activation by oxidatively inactivating PTP1B that physically associated with and deactivated IL-4 receptor. However, ROS were not required for the initiation of IL-4 receptor activation. ROS generated by other cytokine receptors, including those for erythropoietin, tumor necrosis factor-α, or IL-3, also promoted IL-4 signaling. These data indicate that inactivation of receptor-associated PTP activity by cytokine-generated ROS is a physiologic mechanism for the amplification of cytokine receptor activation in both *cis* and *trans*, revealing a role for ROS in cytokine crosstalk.

INTRODUCTION

Interleukin (IL)-4 is an immunomodulatory type I cytokine secreted by activated Th2 lymphocytes, basophils, and mast cells (Haque and Sharma, 2006; Nelms et al., 1999). It executes pleiotropic functions, including induction of Th2 differentiation, immunoglobulin class switching and B cell proliferation, and suppression of Th1 differentiation and macrophage activation, among others (Nelms et al., 1999). IL-4, like many other cytokines, initiates transmembrane signaling by tyrosine phosphorylation of cognate receptors. Protein tyrosine phosphorylation is a tightly regulated, reversible process in which the forward reaction is catalyzed by receptor-associated janus kinases (JAKs) and the reverse reaction by protein tyrosine phosphatases (PTPs) (Haque and Sharma, 2006; Heldin, 1995). In the absence of cytokine engagement, the receptor-associated PTP dominates over the JAK, thereby holding the receptor in an inactive state (Fischer et al., 1991; Haque and Sharma, 2006). Binding of cytokine induces aggregation of receptor chains, leading to the *trans*-phosphorylation of JAKs on signature tyrosine residues. This increases JAKs' catalytic activities that promote the forward reaction, thereby stabilizing the receptor activation (Haque and Sharma, 2006; O'Shea et al., 2002).

This is an established mechanism for receptor activation by a majority of cytokines, including IL-4 (Haque and Sharma, 2006). However, in principle, inactivation of receptor-associated PTP(s) could be an alternate means of receptor activation. As a proof of the principle, we have previously demonstrated that blockade of IL-4 receptor-associated PTP activity by pervanadate (PV) induces receptor activation in the absence of IL-4 binding (Haque et al., 1997). However, PV is a nonphysiologic agent that irreversibly inactivates PTPs. Recent studies have shown that catalytic cysteines of PTPs are reversibly oxidized and inactivated by reactive oxygen species (ROS), including superoxide and hydrogen peroxide (Rhee et al., 2000). ROS are produced by the NAD(P)H oxidase (NOX)/dual oxidase (DUOX) family enzymes in response to cytokine or growth-factor stimulation of cells (Rhee et al., 2000). The NOX/DUOX family is comprised of seven members, NOX1 through NOX5, DUOX1, and DUOX2, each exhibiting cell-type-specific expression (Lambeth, 2004; Lambeth et al., 2007). The catalytic subunits of NOX1, NOX2, NOX3, and NOX4 each form a membrane-integrated heterodimeric complex with the p22phox subunit, which is required for their enzymatic activities (Lambeth et al., 2007). NOX2, the founding member of the NOX/DUOX family, requires the regulatory subunits p47phox, p67phox, p40phox, and Ras-related C3 botulinum toxin substrate (RAC)1/RAC2, whereas NOX1 is regulated by NOX organizer (NOXO)1, NOX activator (NOXA)1, and RAC1 (Lambeth et al., 2007). NOX3- and NOX4-specific regulatory subunits are not known. The long isoforms of NOX5 (NOX5L), DUOX1, and DUOX2 require calcium for their functions (Banfi et al., 2001; Lambeth, 2004; Lambeth et al., 2007).

IL-4 activates two types of receptors. The type I receptor is comprised of the JAK1-bound IL-4Rα and JAK3-bound common gamma chain (γc). Many nonhematopoietic cells that do not express γc and JAK3 utilize the type II receptor in which IL-4Rα associates with JAK2-bound IL-13Rα1 or tyrosine kinase (TYK)2-bound IL-13Rα1 (Nelms et al., 1999). Binding of IL-4 to IL-4Rα induces JAK1-mediated phosphorylation of multiple tyrosine residues in the cytoplasmic region of IL-4Rα. This, in turn, activates two major downstream pathways, insulin-receptor substrate (IRS)-phosphatidylinositol 3-kinase (PI3K) and signal transducer and activator of transcription (STAT)6 (Haque and

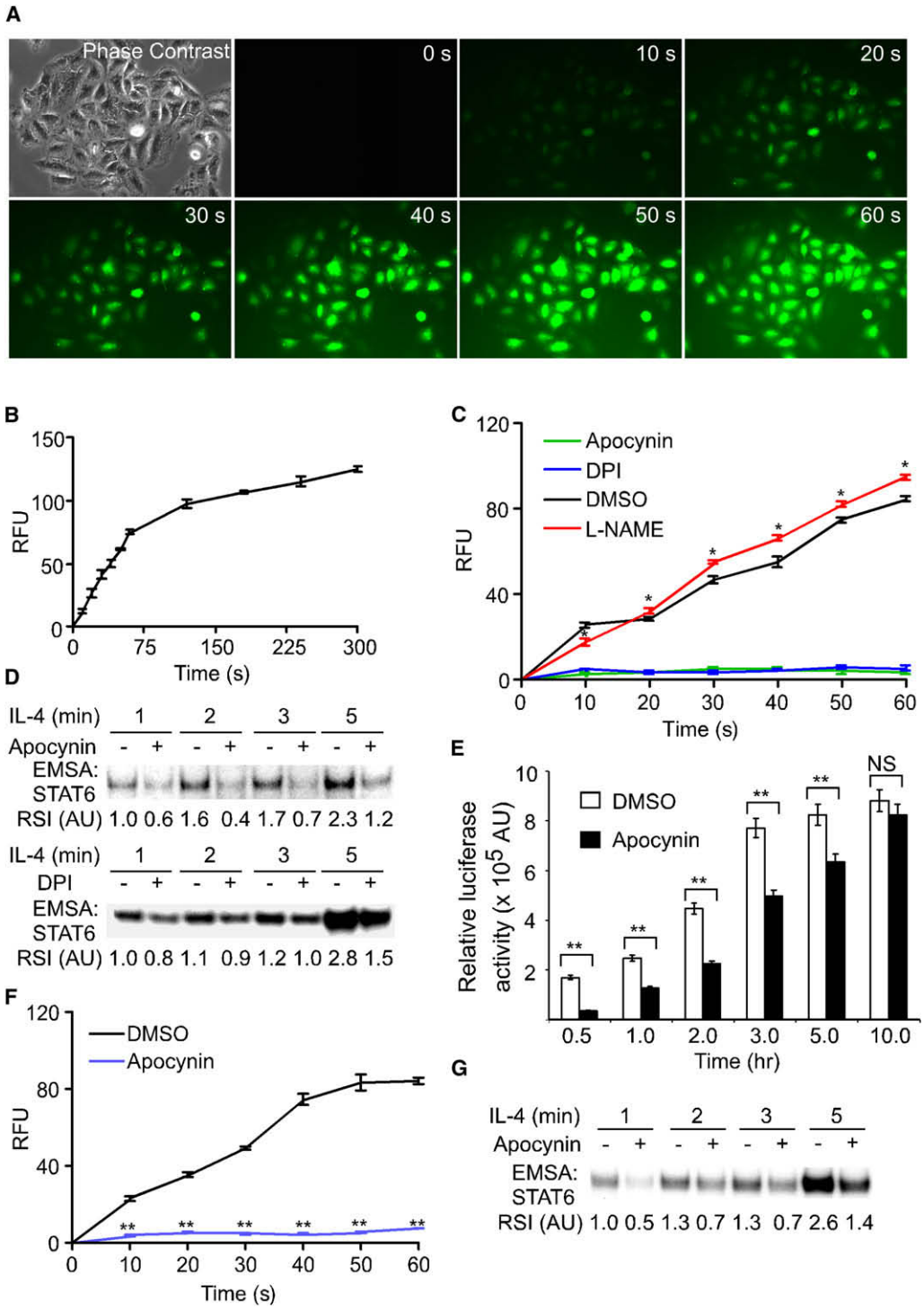

Figure 1. IL-4 Generates ROS that Promote STAT6 Activation and Gene Expression

(A) IL-4 generates ROS in A549 cells. Cells were loaded with 5 μM CM-H_2DCFDA and stimulated with IL-4 (20 ng/ml) under a fluorescence microscope before photography.

(B) ROS generation is rapid in the early phases of IL-4 action. CM-H_2DCFDA-loaded A549 cells were stimulated with IL-4 (20 ng/ml), and fluorescence intensities were quantified. Values in relative fluorescence units (RFU) represent mean ± SE (n = 3).

(C) IL-4 generates ROS by NOX activation. A549 cells were pretreated for 2 hr with apocynin (500 μM), DPI (10 μM), L-NAME (50 μM), or DMSO, and ROS were measured after IL-4 stimulation. RFU represent mean ± SE (n = 3; "*" indicates $p < 0.05$).

(D) Blockade of ROS generation inhibits IL-4-dependent STAT6 activation. A549 cells were pretreated with apocynin, DPI, or DMSO as described above and treated with IL-4 (20 ng/ml) for indicated lengths of time. Cell extracts were subjected to EMSA, and relative signal intensities (RSI) were quantified with ImageQuant software.

Sharma, 2006; Nelms et al., 1999). Because signal transduction, in general, is limited in magnitude and duration, these pathways must be uncoupled by dephosphorylation of the activated receptor.

Here, we demonstrate that activated IL-4 receptor generated ROS by IRS-PI3K-mediated, calcium-dependent and -independent activation of NOX5L and NOX1, respectively. We also show that IL-4 increased intracellular calcium flux, which is required for NOX5L activation. ROS promoted IL-4 receptor activation and subsequent signal transduction by oxidative inactivation of PTP1B, a ubiquitously expressed PTP that deactivated the IL-4 receptor. Further, we provide evidence that ROS generated by other cytokines, like IL-3, erythropoietin (EPO), and tumor necrosis factor (TNF)-α, markedly promoted IL-4 receptor signaling in the same cell, revealing a role for ROS in cytokine crosstalk.

RESULTS

IL-4 Induces ROS Generation, which Promotes Receptor Activation and Signal Transduction

We have previously demonstrated that IL-4 receptor-associated PTP activity is susceptible to inactivation by PV, which is an exogenous oxidant (Haque et al., 1997). Here, we demonstrate that IL-4 stimulation of A549 cells generated endogenous oxidants, ROS, within 10 s (Figures 1A and 1B); ROS reached a peak at ~15 min and declined thereafter (Figure S1 available online). Although the fluorescence probe 5-(and-6)-chloromethyl-2′,7′-dichloro-dihydrofluorescein diacetate (CM-H_2DCFDA) used for ROS measurement can also detect reactive nitrogen species (RNS), pretreatment of cells with an inhibitor of nitric oxide synthase, L-NAME (Kubes et al., 1991), did not reduce IL-4-generated fluorescence intensity, indicating that in response to IL-4, A549 cells did not generate RNS (Figure 1C). To examine whether NOX-family members were involved in IL-4-induced ROS generation, we measured ROS in A549 cells pretreated with diphenylene iodonuim (DPI), an inhibitor of flavoprotein (Cross and Jones, 1986), and apocynin, which inhibits NOX activity (Fu et al., 2006). Both inhibitors completely blocked IL-4-induced ROS generation (Figure 1C), suggesting that NOX-family enzymes were involved in this process. Importantly, these inhibitors substantially reduced IL-4-dependent STAT6 activation as measured by electrophoretic mobility shift assay (EMSA) (Figure 1D) and subsequent gene expression as assessed by STAT6-responsive promoter-driven luciferase activity (Figure 1E) (Haque et al., 2000). Similar observations were made in mouse primary splenocytes (Figures 1F and 1G) and in other cells of both human and mouse origins (data not shown). The specificity of DNA-protein complexes in EMSA was confirmed by competition with an excess of unlabeled DNA probe and by super shift of DNA-protein complex with STAT6-specific antibody (Figure S2). Collectively, these data suggest that IL-4 induces ROS generation in all cell types examined and that ROS induce amplification, but not initiation, of IL-4 signaling.

IL-4 Activates NOX-Family Enzymes through the IRS-PI3K Pathway

To identify the biochemical pathways through which IL-4 induces ROS generation, we used A549 as a model cell line. Binding of IL-4 to its receptor activates IRS-PI3K, STAT6, and rat sarcoma viral oncogene homolog (RAS)-mitogen activated protein kinase (MAPK) (in some cells) pathways (Haque and Sharma, 2006; Nelms et al., 1999). Pretreatment of cells with the JAK inhibitor AG490 (Meydan et al., 1996) or PI3K inhibitors LY294002 and wortmannin (Fukuchi et al., 2000), but not MAPK/extracellular signal-regulated kinase (ERK) kinase (MEK)1 inhibitor U0126 (DeSilva et al., 1998), completely blocked ROS generation by IL-4, suggesting that JAK and PI3K activities are required for IL-4-induced ROS generation (Figure 2A). AG490, LY294002, and wortmannin, but not U0126, also inhibited IL-4-dependent STAT6 activation in A549 cells (Figure 2B), further suggesting that ROS promote IL-4-dependent signal transduction.

To confirm the role of PI3K and determine whether STAT6 has a role in IL-4-induced ROS generation, we undertook the following approach. IL-4 signals A549 cells through the type II receptor (Haque and Sharma, 2006; Nelms et al., 1999). Because the binding of IL-4 to its primary receptor, IL-4Rα, is species specific (Ohara and Paul, 1987), A549 (human) cells did not respond to murine IL-4 (data not shown). IL-13Rα1, which serves as a secondary receptor chain in type II IL-4 receptor complex in A549 cells, does not exhibit species specificity (Nelms et al., 1999). We isolated cDNA of murine IL-4Rα, confirmed its functionality (Figure S3), and generated a mutant receptor (Y500F) deficient in activating the IRS-PI3K pathway (Nelms et al., 1999). When expressed in A549 cells, the wild-type murine IL-4Rα efficiently supported murine IL-4-induced ROS generation, whereas the mutant IL-4Rα (Y500F) failed to do so (Figure 2C), confirming that IRS-PI3K couples the IL-4 receptor to the ROS-generating complex. In addition, inhibition of phosphatase and tensin homolog (PTEN) expression by shRNA (Figure 2D, upper panel) enhanced IL-4-induced ROS generation (Figure 2E) and STAT6 activation (Figure 2D, lower panel) in A549 cells. Further, overexpression of wild-type, but not a catalytically inactive mutant PTEN (C124S) (Myers et al., 1997), inhibited IL-4-induced ROS generation in A549 cells (Figure S4). Taken together, these results confirm the requirement of PI3K activity in IL-4-induced ROS generation.

Murine IL-4Rα did not support the activation of human STAT6 in 293T cells (Figure S3), suggesting that IL-4Rα-STAT6 interaction is also species specific. Consistent with this idea, in response to murine IL-4 treatment, A549 cells expressing the murine IL-4Rα did not activate the endogenous (human) STAT6 (data not shown), but they efficiently supported ROS generation

(E) Blockade of ROS generation inhibits IL-4-dependent gene expression. A549 cells were transfected with 4.0 μg DNA of STAT6-responsive luciferase construct. After 48 hr, cells were pretreated with 500 μM apocynin (or DMSO) for 2 hr and stimulated with IL-4 (20 ng/ml) for indicated lengths of time, and luciferase activity was measured. Luciferase activities in arbitrary units (AU) are plotted as mean ± SE (n = 3; "**" indicates $p < 0.01$; "NS" = not significant).

(F) IL-4 generates ROS by NOX activation in mouse primary splenocytes. Splenocytes were pretreated for 2 hr with apocynin (500 μM) or DMSO, and ROS were measured after IL-4 stimulation. RFU represent mean ± SE, (n = 3; "**" indicates $p < 0.01$).

(G) Blockade of NOX activity inhibits IL-4-dependent STAT6 activation in mouse primary splenocytes. Cells were pretreated with apocynin (500 μM) for 2 hr and treated with IL-4 (20 ng/ml) for indicated lengths of time. Cell extracts were subjected to EMSA, and RSI were quantified.

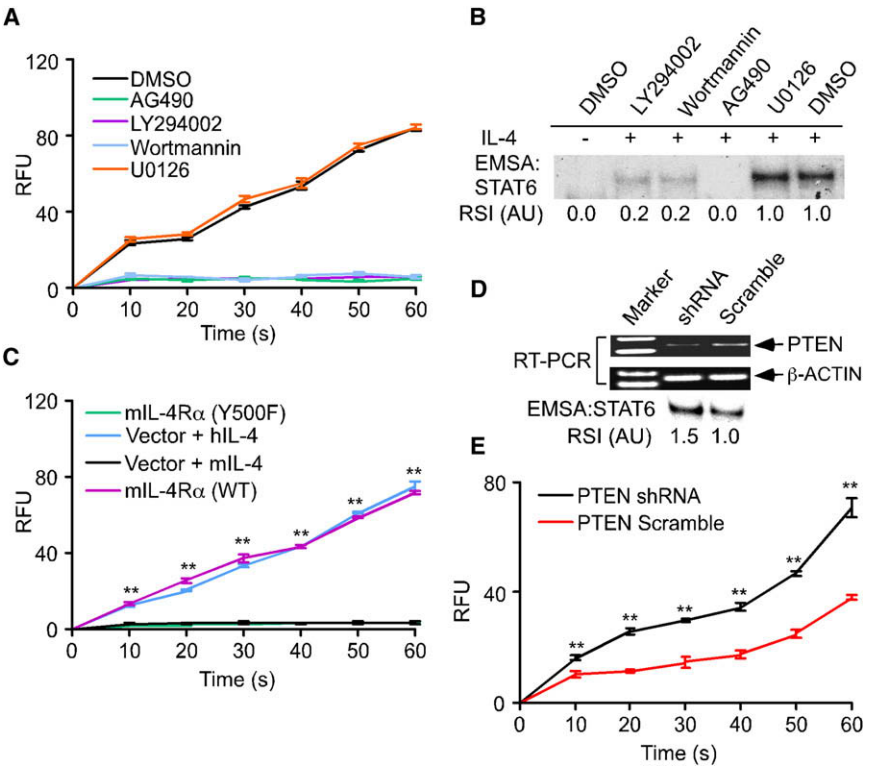

Figure 2. PI3K Activation Is Required for IL-4-Induced ROS Generation

(A) IL-4-induced ROS generation requires JAK and PI3K activities. A549 cells were pretreated with AG490 (50 μM for 6 hr), LY294002 (20 μM for 2 hr), wortmannin (10 nM for 2 hr), U0126 (25 μM for 2 hr), or DMSO, and IL-4-induced ROS generation was measured. RFU are plotted as mean ± SE (n = 3).

(B) Blockade of JAK or PI3K activity inhibits IL-4-induced STAT6 activation. A549 cells were pretreated with the inhibitors described above and stimulated with IL-4 (20 ng/ml) for 5 min. Cell extracts were subjected to EMSA, and RSI were quantified.

(C) PI3K activation is indispensable for IL-4-induced ROS generation. A549 cells were transfected with 1.0 μg of murine wild-type IL-4Rα, murine mutant IL-4Rα (Y500F), or empty vector. After 48 hr, IL-4-generated ROS were measured, and RFU were plotted as mean ± SE (n = 3; "**" indicates $p < 0.01$).

(D) Inhibition of PTEN expression increases IL-4-dependent STAT6 activation. A549 cells were transfected with 4.0 μg of shRNA (or scramble) construct for PTEN. After 48 hr, total RNA was isolated, and steady-state levels of PTEN mRNA were determined by RT-PCR (upper panel). Alternatively, 48 hr posttransfection, cells were stimulated with IL-4 (20 ng/ml) for 5 min. Cell extracts were subjected to EMSA, and RSI were quantified.

(E) Inhibition of PTEN expression increases IL-4-induced ROS generation. A549 cells were transfected as described in (D). After 48 hr, IL-4 generated ROS were measured, and RFU were plotted as mean ± SE (n = 3; "**" indicates $p < 0.01$).

(Figure 2C). Moreover, cycloheximide did not alter IL-4-induced ROS generation in A549 and other cells (data not shown). Taken together, these data clearly indicate that IL-4Rα-mediated ROS generation does not require either STAT6 activation or new protein synthesis.

IL-4 Activates NOX1

The next question was which of the NOX-family members were involved in IL-4-induced ROS generation. We found that NOX1, NOX4, and NOX5L were predominantly expressed in A549 cells (Figure 3A and Figure S5A). Overexpression of NOX1 and NOX5L, but not NOX4, in A549 cells significantly increased IL-4-induced ROS generation (Figure S5B) and also markedly upregulated STAT6 activation (Figure S5C). Further, inhibition of NOX1 expression by shRNA (Figure 3B) compromised IL-4-induced ROS generation (Figure 3C) and STAT6 activation (Figure 3D) in A549 cells. NOX1 activation requires p22phox, NOXA1, NOXO1, and RAC1 (Cheng et al., 2006; Frey et al., 2006; Lambeth et al., 2007). We found that IL-4-induced ROS generation in A549 cells was significantly increased by overexpression of p22phox (Figure S6A) and markedly compromised by either overexpression of a dominant-negative mutant p22phox (P156Q) (Kawahara et al., 2005) or shRNA-mediated inhibition of p22phox expression (Figure S6A). In addition, reconstitution of NOX1 complex in A549 cells by overexpression of NOX1, NOXO1, and NOXA1 significantly increased IL-4-induced ROS generation (Figure S6B). Moreover, IL-4-induced ROS generation was inhibited by overexpression of a dominant-negative mutant RAC1 (T17N) (Cool et al., 1998) (Figure S6C). Further, IL-4 stimulation of A549 cells markedly increased RAC1 activation, which was compromised by inhibition of PI3K activity (Figure S6D). Collectively, these data demonstrate that IL-4 activates NOX1 complex through the IRS-PI3K-RAC1 pathway.

IL-4 Activates NOX5L

Next, we demonstrated the involvement of NOX5L in IL-4-induced ROS generation and STAT6 activation by overexpression (Figures S5B and S5C) and silencing of NOX5L gene in A549 cells (Figures 3B–3D). Because NOX5L activation requires calcium binding (Banfi et al., 2004; Lambeth et al., 2007), we examined whether IL-4-induced ROS generation was dependent on intracellular calcium flux. Pretreatment of A549 cells with BAPTA-AM, a general calcium chelator (Tsien, 1980), or heparin, an inhibitor of inositol 1,4,5-triphosphate (IP3)-receptor-mediated calcium flux (Seuwen and Boddeke, 1995), but not nifedipine, a blocker of L-channel-mediated calcium flux (Reid et al., 1997), markedly inhibited IL-4-induced ROS generation (Figure 4A) and STAT6 activation (Figure 4B). Therefore, it was important to determine whether IL-4 stimulation of cells increased cytoplasmic calcium flux. Using Fluo-4AM (Murata et al., 2004), we detected an increase in cytoplasmic calcium flux by confocal microscopy within 5 s of IL-4 stimulation of A549 cells; it

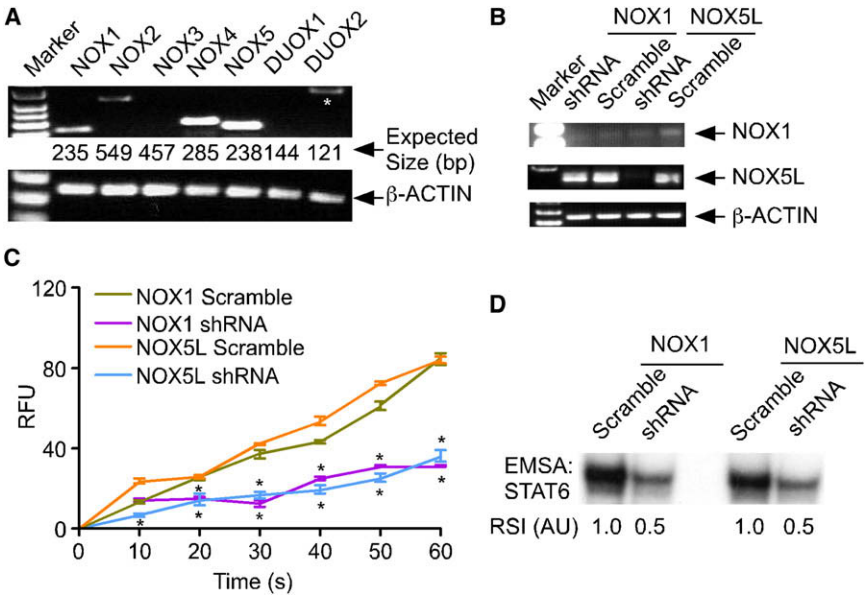

Figure 3. NOX1 and NOX5L Are Involved in IL-4-Induced ROS Generation

(A) Different NOX genes are expressed in A549 cells. Total RNA from cells was used for RT-PCR with NOX-specific primers (upper panel) or for β-actin (lower panel). The expected sizes (bp) of PCR products are indicated below, and nonspecific products are indicated by asterisks.

(B) Inhibition of NOX1 and NOX5L expression by shRNA. A549 cells were transfected with 4.0 μg of shRNA constructs for NOX1, NOX5L, or their scramble versions. After 48 hr, steady-state levels of NOX1 and NOX5L mRNAs were determined by RT-PCR.

(C) Inhibition of NOX1 and NOX5L expression reduces IL-4-induced ROS generation. A549 cells were transfected as in (B). After 48 hr, IL-4-generated ROS were measured, and RFU were plotted as mean ± SE (n = 3; "*" indicates $p < 0.05$).

(D) Inhibition of NOX1 and NOX5L expression reduces IL-4-dependent STAT6 activation. A549 cells were transfected as in (B). After 48 hr, cells were stimulated with IL-4 (20 ng/ml) for 5 min. Cell extracts were subjected to EMSA, and RSI were quantified.

continued to increase for ~180 s and reached a plateau thereafter (Figures 4C and 4D). The kinetics of this calcium flux correlated with those of IL-4-induced ROS generation (Figure 1B).

To examine the role of phospholipase C (PLC)γ, which catalyzes the production of IP3 and diacylglycerol (DAG) in IL-4-induced NOX5L activation, we pretreated A549 cells with PLCγ inhibitor U73122 (Stam et al., 1998) or inhibitors of DAG-dependent protein kinase C (PKC), calphostin C (Jarvis et al., 1994) and Go6976 (Gschwendt et al., 1996), and found that IL-4-induced ROS generation was significantly inhibited (Figure S7). Further, shRNA-mediated inhibition of PLCγ1 and PLCγ2 expression (Figure 4E, upper panel) reduced IL-4-induced ROS generation (Figure 4F) and STAT6 activation (Figure 4E, lower panel) in A549 cells. Collectively, these results demonstrate that activated IL-4 receptor induces an intracellular calcium flux via the IRS-PI3K-PLCγ pathway that probably induced DAG- and calcium-dependent PKC-mediated activation of NOX5L to generate ROS in A549 cells.

The mouse genome does not possess a gene encoding NOX5, but it does possess genes that encode DUOX1 and DUOX2 (Lambeth, 2004; Lambeth et al., 2007). We found that mouse $CD4^+$ naive T cells, but not mouse embryonic fibroblasts (MEFs), expressed DUOX1 (Figure S8A) that requires calcium for activation (Lambeth, 2004). However, BAPTA-AM and heparin failed to inhibit IL-4-induced ROS generation in mouse T cells (Figure S8B) and in MEFs (as expected) (Figure S8C). Because NOX1 was predominantly expressed in both these cell types, IL-4-induced ROS generation was probably mediated by NOX1 in these cells.

PTP1B Negatively Regulates IL-4 Signaling

To understand the biochemical basis of ROS-mediated amplification of IL-4 signaling, we wished to examine whether ROS generated by activated IL-4 receptor oxidatively inactivate the IL-4 receptor-associated PTP activity. Prior to addressing this question, it was necessary to know the molecular identity of the PTP that deactivates IL-4 receptor. Previously, we and others have identified SHP-1 and CD45 that are exclusively expressed in hematopoietic cells as negative regulators of IL-4 signaling (Haque et al., 1998; Yamada et al., 2002). Because IL-4 induced ROS generation in all cell types examined, we sought to identify a ubiquitously expressed PTP that deactivates IL-4 receptor. Screening of a panel of such PTPs by overexpression in 293T cells identified PTP1B as a potential candidate that substantially inhibited IL-4-dependent STAT6 activation (Figure S9A). Consistently, overexpression of wild-type, but not catalytically inactive mutant PTP1B (C215S), markedly inhibited IL-4-dependent STAT6 activation (Figure S9B) and subsequent gene expression in 293T cells (Figure S9C). These observations were confirmed in immortalized embryonic fibroblasts derived from *Ptpn1*$^{-/-}$ mice (Buckley et al., 2002; Elchebly et al., 1999), which exhibited substantial increases in magnitude and duration of IL-4-induced activation of STAT6 (Figure 5A). Further, IL-4-dependent STAT6 activation was markedly inhibited after insertion of PTP1B in PTP1B-deficient MEFs (Figure 5B). Moreover, IL-13 that utilizes the type II IL-4 receptor for cell signaling (Nelms et al., 1999) also substantially increased STAT6 activation in *Ptpn1*$^{-/-}$ MEFs compared with wild-type MEFs (Figure S9D).

PTPs may exhibit functional redundancy in the regulation of cytokine signaling pathways. SHP-1 and CD45 inhibit IL-4 signaling in hematopoietic cells (Haque et al., 1998; Yamada et al., 2002); therefore, it was important to know whether PTP1B negatively regulates IL-4 signaling in hematopoietic cells. As shown in Figure 5C, IL-4-dependent STAT6 activation was markedly increased in primary splenocytes derived from *Ptpn1*$^{-/-}$ mice. Importantly, PTP1B deficiency also increased IL-4-induced ROS generation in both MEFs (Figure 5D) and splenocytes (Figure 5E). Further, insertion of PTP1B in PTP1B-deficient MEFs significantly reduced IL-4-induced ROS generation (Figure 5D). PTP1B deficiency also increased ROS generation by IL-4 in mouse primary macrophages, mast cells, and T cells and by IL-13 in MEFs, splenocytes, and macrophages

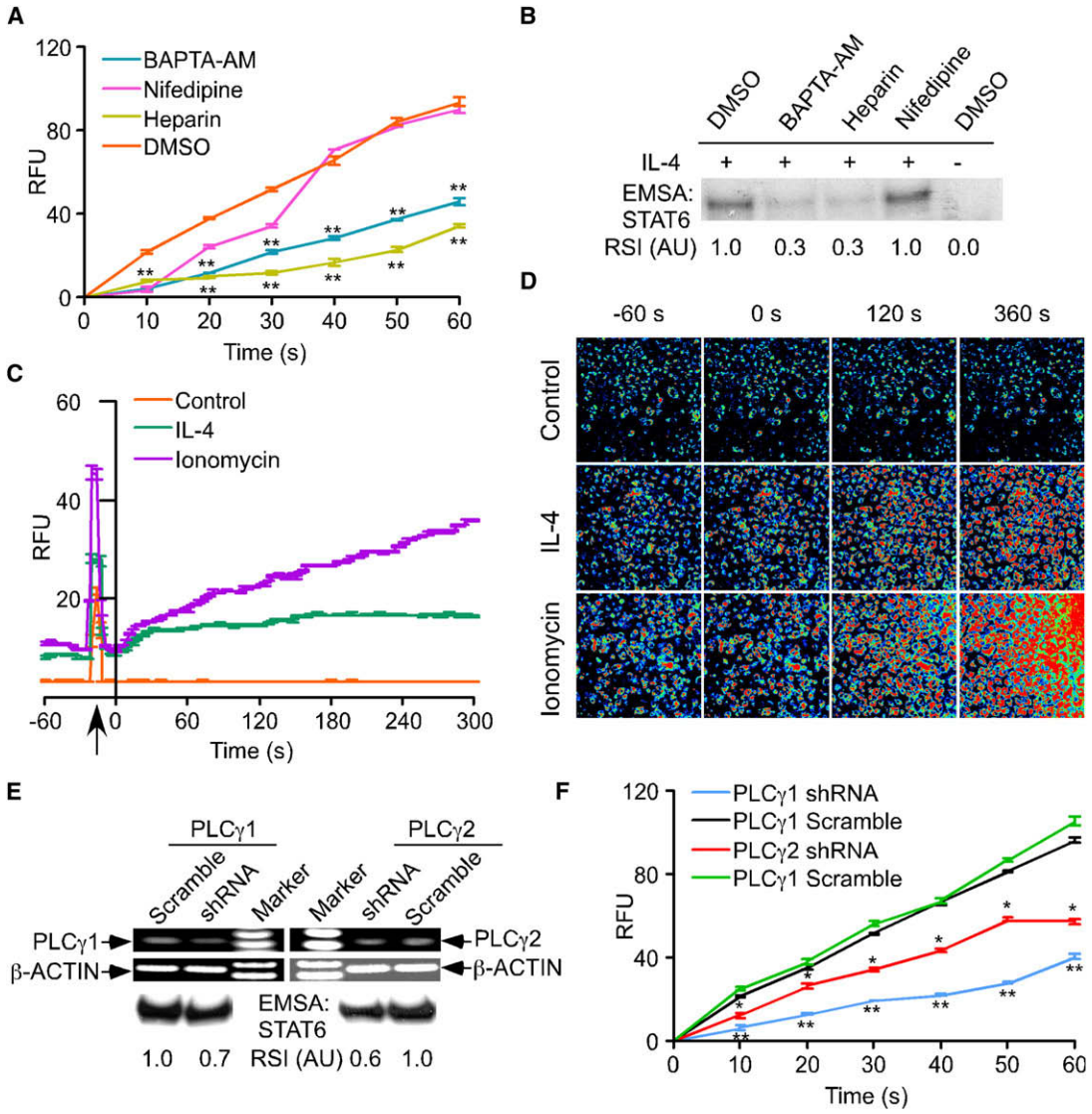

Figure 4. IL-4 Induces Calcium Flux that Increases ROS Generation

(A) IL-4-induced ROS generation is inhibited by blocking IP3-receptor-mediated calcium release. A549 cells were treated for 2 hr with BAPTA-AM (30 μM), heparin (1 μM), nifedipine (0.1 nM), or DMSO, and IL-4-generated ROS measured in RFU are plotted as mean ± SE (n = 3; "**" indicates $p < 0.01$).

(B) Inhibition of IP3-receptor-mediated calcium release compromises IL-4-dependent STAT6 activation. A549 cells were pretreated as in (A) and treated with IL-4 (20 ng/ml) for 5 min. Cell extracts were subjected to EMSA, and RSI were quantified.

(C) IL-4-stimulation increases cytoplasmic calcium flux. A549 cells were loaded with 1 μM Fluo4-AM, and changes in cytoplasmic calcium levels were measured with live-cell confocal microscopy. The arrow indicates the time when the medium was replaced by fresh medium containing 20 ng/ml of IL-4 or 1 μM of ionomycin (as positive control). The experiment was performed five times, and data of one representative experiment are shown.

(D) IL-4-stimulation increases cytoplasmic calcium flux. A549 cells were processed as in (C), and confocal microscopic pictures were taken. The experiment was performed five times, and data of one representative experiment are shown.

(E) Inhibition of PLCγ1 or PLCγ2 expression by shRNA reduces IL-4-dependent STAT6 activation. A549 cells were transfected with 4.0 μg of shRNA or scramble construct for PLCγ1 or PLCγ2. After 48 hr, PLCγ1 and PLCγ2 transcript levels were determined by RT-PCR (upper panel). Alternatively, 48 hr posttransfection, cells were stimulated with IL-4 for 5 min. Cell extracts were subjected to EMSA, and RSI were quantified.

(F) Inhibition of PLCγ1 or PLCγ2 expression by shRNA reduces IL-4-induced ROS generation. A549 cells were transfected as in (E). After 48 hr, IL-4-generated ROS were measured, and RFU were plotted as mean ± SE (n = 3; "*" indicates $p < 0.05$; "**" indicates $p < 0.01$).

(Figure S10). Collectively, these data demonstrate that PTP1B functions as a nonredundant negative regulator of IL-4 and IL-13 signaling in hematopoietic and nonhematopoietic cells.

Next, we asked whether PTP1B deficiency favors the differentiation of naive $CD4^+$T cells to Th2 effector cells. Highly purified $CD44^{lo}$ naive $CD4^+$ T cells were obtained from lymph nodes of *Ptpn1*$^{+/+}$ and *Ptpn1*$^{-/-}$ mice by cell sorting and subsequently stimulated with anti-CD3 and anti-CD28 in the presence of irradiated T cell-depleted splenocytes. We included cytokines and antibodies in the culture to induce Th1 or Th2 differentiation. As shown in Figure 5F, enhanced IL-4 producing Th2 cells were found in PTP1B-deficient $CD4^+$ T cells. Enhanced IL-4

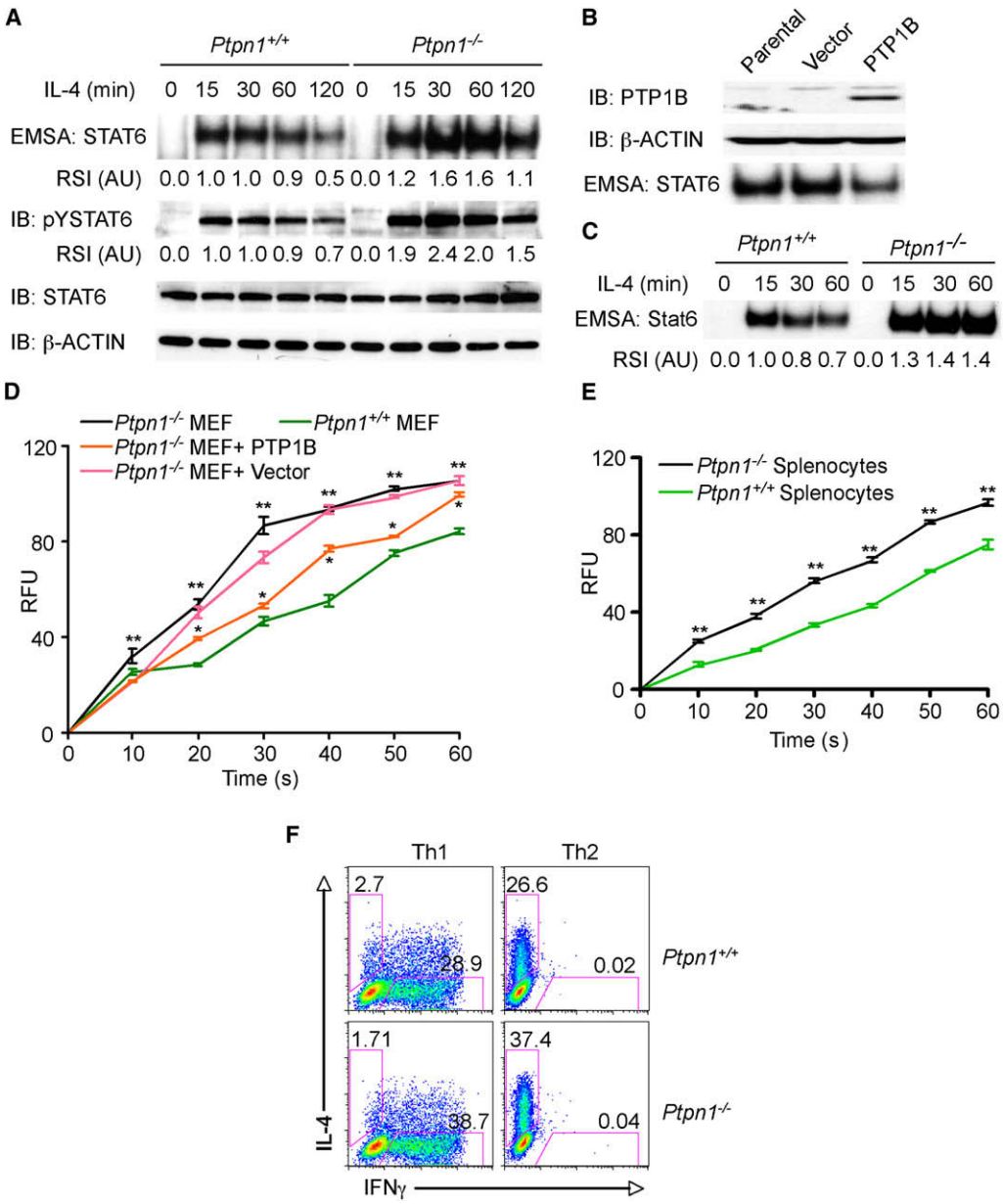

Figure 5. PTP1B Negatively Regulates IL-4 Signaling

(A) PTP1B deficiency increases IL-4-dependent STAT6 activation in MEFs. PTP1B-deficient (*Ptpn1*$^{-/-}$) and wild-type (*Ptpn1*$^{+/+}$) MEFs (immortalized) were treated with IL-4 (20 ng/ml) for the indicated lengths of time, cell extracts were subjected to EMSA and immunoblot analysis (with anti-phospho-Tyrosine641-STAT6), and RSI were quantified. Immunoblot analyses with anti-STAT6 and anti-β-actin served as controls.

(B) Reintroduction of PTP1B to *Ptpn1*$^{-/-}$ MEFs reduces IL-4-dependent STAT6 activation. Immortalized *Ptpn1*$^{-/-}$ MEFs were stably transfected with either empty vector or PTP1B, and clones were selected in the presence of hygromycin B. Selected pools were treated with IL-4 (20 ng/ml) for 30 min, and cell extracts were subjected to immunoblot analyses and EMSA.

(C) PTP1B deficiency increases IL-4-dependent STAT6 activation in mouse primary splenocytes. Splenocytes from *Ptpn1*$^{+/+}$ and *Ptpn1*$^{-/-}$ mice were treated with IL-4 (20 ng/ml) for the indicated lengths of time, cell extracts were subjected to EMSA, and RSI were quantified.

(D) PTP1B deficiency increases IL-4-induced ROS generation in immortalized MEFs. MEFs derived from *Ptpn1*$^{+/+}$ and *Ptpn1*$^{-/-}$ mice and representative clones of *Ptpn1*$^{-/-}$ MEFs stably transfected with PTP1B (or empty vector) were treated with IL-4 for indicated lengths of time, and ROS were measured. RFU are plotted as mean ± SE (n = 3; "*" indicates $p < 0.05$; "**" indicates $p < 0.01$).

(E) PTP1B deficiency increases IL-4-induced ROS generation in mouse primary splenocytes. Splenocytes isolated from *Ptpn1*$^{+/+}$ and *Ptpn1*$^{-/-}$ mice were stimulated with IL-4 for indicated lengths of time, and ROS were measured. RFU are plotted as mean ± SE (n = 3; "**" indicates $p < 0.01$).

(F) PTP1B deficiency increases the number of IL-4-producing CD4$^+$ T cells. Naive CD4$^+$ T cells were purified from lymph nodes of *Ptpn1*$^{+/+}$ and *Ptpn1*$^{-/-}$ mice and cultured with anti-CD3 and anti-CD28 plus T cell-depleted syngenic irradiated spleen cells as a source of antigen-presenting cells, in a ratio of 1:5, for 72 hr under conditions inducing Th1 or Th2 differentiation. Intracellular IL-4 and IFN-γ expression was determined by flow cytometry after restimulation with anti-CD3 and anti-CD28 for 6 hr.

production was also observed when T cells were stimulated in Th-neutral condition (data not shown). These data suggest that PTP1B negatively controls Th2 differentiation of naive $CD4^+$ T cells in vitro. We also noted that PTP1B-deficient $CD4^+$ T cells produced more IFN-γ when stimulated under Th1 condition. Th1 differentiation is controlled by IL-12 and IFN-γ signaling (Nelms et al., 1999). PTP1B binds to and dephosphorylates JAK2, thereby attenuating IFN-γ signaling (Myers et al., 2001). Although PTP1B-mediated downregulation of IL-12 signaling has not been directly demonstrated, JAK2 and TYK2, which are required for IL-12-mediated cell signaling (Haque and Sharma, 2006), are shown to be potential substrates for PTP1B. Therefore, it was not unexpected that PTP1B deficiency would increase the number of IFN-γ producing cells under Th1-skewed condition (Figure 5F).

PTP1B Deactivates IL-4 Receptor

Next, to determine whether PTP1B dephosphorylates IL-4 receptor, we used a chimeric receptor, EPOR-IL-4Rα, composed of the extracellular and transmembrane domains of the murine EPO receptor and the cytoplasmic domain of the human IL-4Rα (Figure S11A). When coexpressed with STAT6 in 293T cells (which do not express endogenous functional STAT6), this receptor becomes activated upon EPO binding and induces STAT6 activation (Haque et al., 2000). PTP1B substantially inhibited EPO-dependent tyrosine phosphorylation of EPOR-IL-4Rα and subsequent activation of STAT6 in 293T cells (Figure 6A), suggesting that PTP1B may interact with IL-4Rα, JAK1, or STAT6. However, a previous study has shown that JAK1 does not bind to PTP1B (Myers et al., 2001). To determine whether PTP1B binds to IL-4Rα and/or STAT6, either wild-type PTP1B or substrate-trapping mutant PTP1B (D181A) (Flint et al., 1997) was coexpressed with EPOR-IL-4Rα and/or STAT6 in 293T cells. Employing conventional coimmunoprecipitation technique, we could not detect physical association of PTP1B with either EPOR-IL-4Rα or STAT6 (data not shown). However, when cell lysates were prepared in the presence of the chemical crosslinking agent dithio[succimidyl propionate] (DSP) (Maiti et al., 2005), PTP1B was found to form a complex with IL-4Rα, but not STAT6 (Figure 6B), suggesting that the interaction between PTP1B and IL-4Rα was weak and dynamic in nature. Further, using deletion mutants of EPOR-IL-4Rα (Figure S11B), we mapped a PTP1B-interacting region in IL-4Rα to a region encompassing the STAT6-docking sites (Nelms et al., 1999) (Figure S11C).

Bioluminescence resonance energy transfer (BRET) is a powerful tool for the detection of weak and dynamic protein-protein interactions in live cells (Pfleger and Eidne, 2006). Employing this technique, we detected an interaction between PTP1B (D181A) and IL-4Rα, even in the absence of IL-4 stimulation; the interaction was increased by IL-4 stimulation of cells (Figure 6C). These results confirmed the in vitro crosslinking data indicating that PTP1B physically associates with IL-4Rα.

ROS Inactivate PTP1B by Oxidation of Its Catalytic Cysteine and Mediate Cytokine Crosstalk

ROS-mediated oxidative inactivation of PTP1B has been demonstrated both in vitro (Salmeen et al., 2003; van Montfort et al., 2003) and in vivo by insulin and epidermal growth factor (EGF) (Lee et al., 1998; Mahadev et al., 2001; Meng et al., 2002). Because we found that IL-4 induced ROS generation

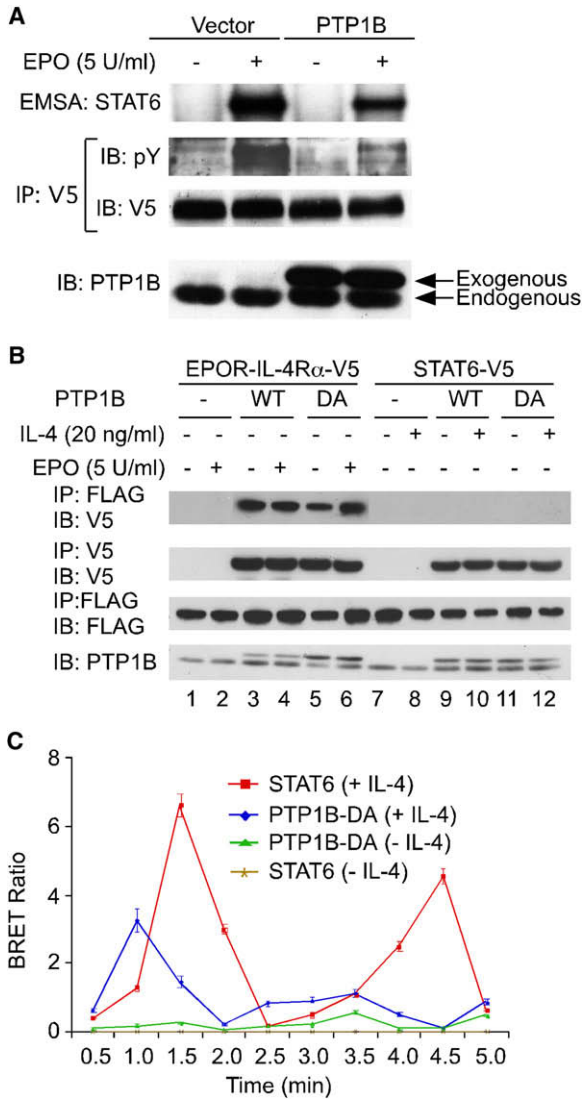

Figure 6. PTP1B Binds to and Dephosphorylates IL-4Rα

(A) PTP1B deactivates IL-4Rα. 293T cells were transfected with 50 ng of STAT6 and 5.0 μg of chimeric EPOR-IL-4Rα–V5, along with 5.0 μg of PTP1B or vector. After 48 hr, cells were treated with EPO (5 U/ml) for 5 min, and cell extracts were subjected to EMSA. Immunoprecipitates derived from 1.0 mg proteins or 50 μg proteins (cell lysate) were used for immunoblotting. The experiment was repeated two times, and similar results were obtained.

(B) PTP1B physically associates with the cytoplasmic domain of IL-4Rα. In lanes 1 to 6, 293T cells were transfected with EPO-IL-4Rα-V5 (2.0 μg), untagged STAT6 (2.0 μg), and 4.0 μg of wild-type PTP1B-FLAG, mutant PTP1B (D181A)-FLAG, or empty vector. In lanes 7 to 12, cells were transfected with 2.0 μg of STAT6-V5 and 4.0 μg wild-type PTP1B-FLAG, mutant PTP1B (D181A)-FLAG, or empty vector. After 48 hr, cells were treated with EPO (5 U/ml) or IL-4 (20 ng/ml) for 5 min. Cell lysates were prepared in the presence of DSP and immunoprecipitated (IP) with anti-FLAG, decrosslinked, and subjected to immunoblot analyses along with decrosslinked total lysates.

(C) PTP1B interacts with IL-4Rα in live cells. For BRET assay, 293T cells were transfected with 1.0 μg of the donor plasmid pIL-4Rα-LUC-N3 and 3.0 μg of an acceptor plasmid $pGFP^2$-N2 (empty vector), STAT6-GFP^2-N2, or PTP1B-D181A-GFP^2-N2 with Lipofectamine 2000 (Invitrogen). After 48 hr, cells were used for BRET assay, and the calculated BRET ratios are plotted as mean ± SE (n = 3).

(Figure 1) and PTP1B deactivated IL-4 receptor (Figure 6A), it was important to examine whether IL-4-generated ROS could cause oxidative inactivation of PTP1B. Using a monoclonal antibody against oxidized PTP-active site (Persson et al., 2004), we observed a time-dependent oxidation of the catalytic cysteine 215 of PTP1B in A549 cells after stimulation with IL-4 (Figure 7A) or IL-13 (Figure 7B). Further, pretreatment of these cells with apocynin or LY294002 that completely inhibited IL-4-induced ROS generation (Figures 1C and 2A) markedly reduced the oxidation of PTP1B (Figure 7C). Moreover, shRNA-mediated reduction of NOX1 or NOX5L expression, which significantly decreased IL-4-induced ROS generation (Figure 3C), substantially inhibited IL-4-induced oxidation of PTP1B in A549 cells (Figure 7D). IL-4 also induced a time-dependent oxidation of PTP1B in primary mouse splenocytes (Figure 7E) and bone marrow-derived macrophages (Figure 7F). These results clearly demonstrate that ROS-mediated amplification of IL-4 (or IL-13) signaling was, in part, due to oxidative inactivation of PTP1B, in both primary and immortalized cells.

Under physiologic settings, multiple cytokines may act on a single cell that expresses the cognate receptors. Because ROS are small and diffusible radicals or molecules, oxidative inactivation of PTP1B by other cytokine-generated ROS may amplify the activation of IL-4 receptor in the same cell. To examine this possibility, we expressed in A549 cells the mutant murine IL-4Rα (Y500F) that did not generate ROS (Figure 2C) but supported STAT6 activation in response to murine IL-4 stimulation (Figure 7G). As shown in Figure 7G, a simultaneous stimulation of these cells with EPO and murine IL-4 substantially increased STAT6 activation. EPO did not activate STAT6 (Figure 7G), but it induced ROS generation in these cells (Figure S12A). These results suggest that EPO-generated ROS can act in *trans* to promote IL-4 signaling in the same cell. Further, to examine whether EPO or other cytokines can promote IL-4 signaling through its endogenous receptor, we pretreated A549 cells with EPO or TNF-α and then treated them with IL-4 in the presence or absence of PI3K inhibitor LY294002. Figure 7H shows that both EPO and TNF-α markedly promoted the activation of endogenous IL-4 receptors in A549 cells. Similar observations were made in mouse primary splenocytes in which ROS generated by IL-3 or TNF-α (Figures S12B and S12C) markedly increased IL-4-dependent STAT6 activation (Figures 7I and 7J). Of note is the fact that LY294002 completely blocked EPO- and TNF-α-induced ROS generation in A549 cells but failed to completely inhibit IL-3- and TNF-α-induced ROS generation in primary splenocytes (Figure S12), suggesting that IL-3 and TNF-α may also induce ROS generation by PI3K-independent mechanism(s). Importantly, the amounts of IL-3- or TNF-α-generated ROS correlated with the extents of STAT6 transactivation (Figures 7G–J).

Collectively, these results demonstrate that ROS produced by activation of other cytokine receptors were able to promote the activation of IL-4 receptor in the same cell, suggesting that ROS can serve as a physiologic mediator of crosstalk between different cytokine receptors (Figure S13).

DISCUSSION

In this study, we have demonstrated that immediately after IL-4 engagement, activated receptor produced ROS that, in turn, increased the magnitudes of receptor activation and consequent signal transduction in all IL-4-responsive cells examined, in the absence of de novo protein synthesis and STAT6 activation. Subsequently, undertaking multiple complementary approaches, we have demonstrated that IL-4 induced the activation of NOX1 and NOX5L through PI3K-RAC1 and PI3K-PLCγ, respectively.

The mechanisms of NOX1 activation are characterized in a number of cell types. NOX1 requires p22phox, NOXA1, RAC1, and NOXO1 for activation (Lambeth et al., 2007). Typically, NOXO1 is recruited to NOX1-p22phox complex, to which NOXA1 is recruited by activated RAC1 (Lambeth et al., 2007). An earlier report showed that IL-4 activates RAC1 in human keratinocytes (Wery-Zennaro et al., 2000), but it is not known whether IL-4-activated RAC1 induces NOX1 activation. Our results demonstrate that phosphorylation of specific tyrosine (Y497 in human and Y500 in mouse) in IL-4Rα that recruits IRS-PI3K was required for IL-4-dependent ROS generation by NOX1 and NOX5L (in human cells). PI3K-dependent regulation of NOX-mediated ROS generation has previously been demonstrated in EGF- and TNF-α-stimulated cells (Frey et al., 2006; Park et al., 2004). We found that IL-4-activated PI3K-dependent RAC1 activation was indispensable for ROS generation in A549 cells, suggesting that IL-4 activates RAC1 through PI3K, and RAC1 is involved in ROS generation by NOX1, as dominant-negative mutant RAC1 (T17N) compromised ROS generation by IL-4.

IL-4-dependent ROS generation was also significantly reduced by inhibitors of cytoplasmic calcium flux, suggesting that calcium flux was required for IL-4-induced NOX5L activation. It was not known whether IL-4 induced calcium flux. Using Fluo-4AM, whose fluorescence intensity increases >100-fold upon calcium binding (Harkins et al., 1993), we demonstrated that IL-4 induced an immediate cytoplasmic calcium flux in A549 cells. IL-4-induced ROS generation was inhibited by shRNA or small-molecule inhibitor of PLCγ1 and PLCγ2. Two studies have previously demonstrated the role for PLCγ1 in IL-4 signaling (Ikizawa et al., 1994; Ikizawa and Yanagihara, 2000), whereas another report has implicated a role of phosphatidylcholine-specific PLC, but not PLCγ, in IL-4 signaling (Zamorano et al., 2003). This discrepancy may be due to the latter study's use of mouse cells, which do not express NOX5 (Banfi et al., 2001). Interestingly, IL-4-dependent ROS generation was markedly reduced by the inhibition of DAG-dependent PKCs. A recent study showed that activation of NOX5L is regulated by unidentified PKC-mediated phosphorylation of a serine and a threonine located in the FAD-binding domain of NOX5 (Jagnandan et al., 2007). Previous studies have focused on DAG- and calcium-independent PKC-mediated regulation of IL-4 signaling (Duran et al., 2004; Ho et al., 1994). Our results suggest a role for classical PKCs that depend on both DAG and calcium for activation in IL-4-mediated cell signaling. The mouse genome does not contain a gene encoding NOX5, but it does contain genes encoding DUOX1 and DUOX2, which require calcium for activation. We noted that mouse T cells, but not MEFs, expressed DUOX1; however, calcium blockers did not inhibit IL-4-induced ROS generation, suggesting that IL-4-induced ROS generation was catalyzed by NOX1, which was predominantly expressed in both the mouse cell types. Further studies are necessary to confirm whether IL-4 induces calcium flux and whether it is required for

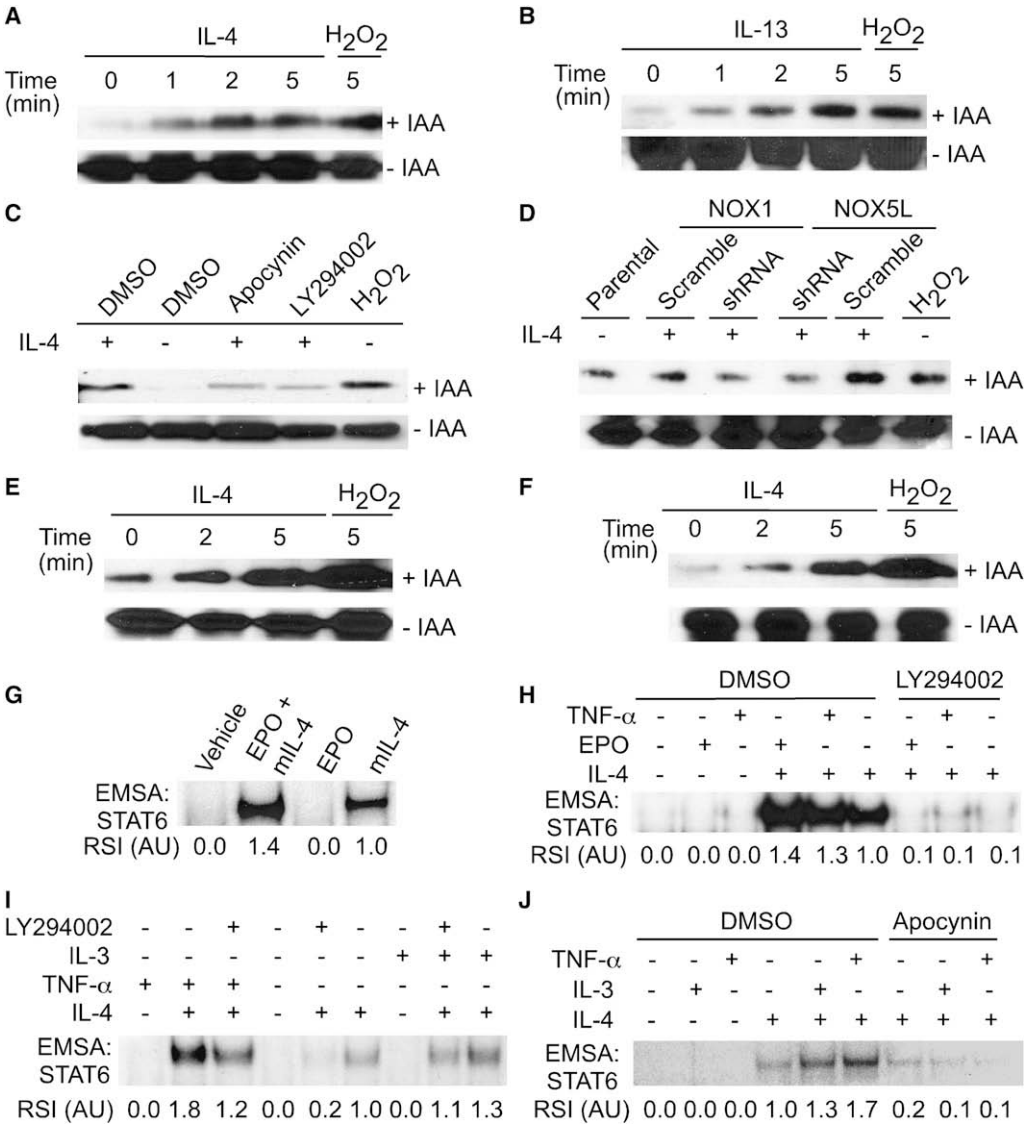

Figure 7. ROS Induce PTP1B Oxidation and Cytokine Crosstalk

(A and B) Oxidation of PTP1B in IL-4- or IL-13-stimulated A549 cells. Cells were treated with 20 ng/ml of IL-4 (A) or 10 ng/ml of IL-13 (B) for indicated lengths of time, with 3 mM H_2O_2 (positive control) for 5 min, or were left untreated. Cell lysates were prepared in the presence (upper panel) or absence (lower panel) of IAA and immunoprecipitated with anti-PTP1B, and the immune complexes were subjected to immunoblot analysis with a monoclonal antibody that recognizes oxidized PTP1B.

(C) Blockade of ROS generation inhibits PTP1B oxidation in IL-4-stimulated cells. A549 cells were treated with 500 μM apocynin, 20 μM LY294002, or DMSO for 2 hr prior to measurement of IL-4-induced oxidation of PTP1B. The upper and lower panels represent results derived from cell lysates prepared in the presence and absence of IAA, respectively. The experiment was repeated two times, and similar results were obtained.

(D) Inhibition of NOX1 or NOX5L expression reduces IL-4-induced PTP1B oxidation. A549 cells were transfected with 4.0 μg of shRNA or scramble constructs for NOX1 or NOX5L. After 48 hr, cells were treated with IL-4 (20 ng/ml) or H_2O_2 (3 mM) for 5 min or left untreated. Cell lysates were prepared in the presence or absence of IAA, and PTP1B oxidation was measured.

(E and F) IL-4-generated ROS induce PTP1B oxidation in mouse primary hematopoietic cells. Splenocytes (E) and bone marrow-derived macrophages (F) were stimulated with IL-4 for indicated lengths of time or with 3 mM H_2O_2 for 5 min. Cell lysates were prepared in the presence or absence of IAA, and PTP1B was oxidation measured.

(G) EPO-generated ROS promote IL-4-dependent STAT6 activation. A549 cells were transfected with 1.0 μg of murine IL-4Rα (Y500F), along with 3.0 μg of murine STAT6 plasmid. After 48 hr, cells were treated for 5 min with EPO (5U/ml) and murine IL-4 (20 ng/ml), either singly or in combination. Cell extracts were subjected to EMSA, and RSI were quantified.

(H) TNF-α- and EPO-generated ROS promote endogenous IL-4 receptor activation in A549 cells. Cells pretreated with LY294002 (20 μM) or DMSO for 2 hr were stimulated for 3 min with EPO (5U/ml) or TNF-α (10 ng/ml), followed by treatment with human IL-4 (20 ng/ml) for 2 min. Cell extracts were subjected to EMSA, and RSI were quantified.

(I and J) TNF-α- and IL-3-generated ROS promote endogenous IL-4 receptor activation in mouse primary splenocytes. After pretreatment for 2 hr with LY294002 (20 μM) (I) or apocynin (500 μM) (J), cells were treated for 3 min with TNF-α (10 ng/ml) or IL-3 (10 ng/ml), followed by treatment with mouse IL-4 (20 ng/ml) for 2 min. Cell extracts were subjected to EMSA, and RSI were quantified.

DUOX1- or DUOX2-catalyzed ROS generation in other murine cell types.

We found that IL-4-generated ROS promoted IL-4-dependent signal transduction and gene expression. We have demonstrated that as an underlying mechanism, PTP1B physically interacted with IL-4Rα and deactivated it, and IL-4-generated ROS inactivated its catalytic cysteine 215 by oxidation in both hematopoietic and nonhematopoietic cells. Because IL-13Rα1, the second chain of type II IL-4 receptor, constitutively associates with JAK2 or TYK2, PTP1B-mediated attenuation of type II IL-4 receptor activation may also be attributed to PTP1B-catalyzed deactivation of JAK2 or TYK2 (Myers et al., 2001).

Both oxidative inactivation and genetic inactivation of PTP1B were found to upregulate IL-4 receptor activation and signal transduction. However, the former is a reversible and physiologic process, whereas the latter is a nonphysiologic and irreversible depletion of PTP1B function. PTP1B inactivation by ROS occurs locally at the site of IL-4 receptor activation and its immediate vicinity, whereas genetic inactivation of PTP1B occurs globally, and this unleashes PTP1B-dependent restraints on all the signaling pathways that are regulated by PTP1B under normal physiologic conditions. As a consequence, an in vitro differentiation of PTP1B-deficient naive Th cells can be expected to be skewed to both Th1 and Th2 lineages, given that PTP1B functions as a negative regulator of IL-4 (the current study) and IFN-γ (and probably IL-12) signaling pathways (Myers et al., 2001).

Our data also revealed that PTP1B played a nonredundant role in hematopoietic cells in which both SHP-1 and CD45 are found to downregulate IL-4-dependent signal transduction (Haque et al., 1998; Yamada et al., 2002). Therefore, it remains to be examined whether SHP-1 and CD45 are also oxidatively inactivated by IL-4-generated ROS, given that the catalytic cysteine is conserved in all PTPs and susceptible to oxidation by ROS (Rhee et al., 2000).

ROS are small, diffusible radicals or molecules that inactivate PTPs, including PTP1B (Rhee et al., 2000). Using IL-4 as a model cytokine, we have uncovered a cellular mechanism underlying the homeostatic control of cytokine receptor activation and signal transduction by addressing how an activated cytokine receptor induced ROS generation by activating NOX enzymes to promote the receptor's own activation as well as the activation of other cytokine receptors in the same cell. ROS-mediated cytokine signaling crosstalk may be dependent on the proximity of the different cytokine (or growth-factor) receptors and their susceptibility to regulation by oxidative inactivation of common PTPs. Another level of regulation may be provided by the specificity and abundance of the antioxidant proteins utilized by different receptors for elimination of cytokine-generated ROS, thus allowing the regeneration of reversibly inactivated PTPs and the restoration of normal homeostasis of cellular cytokine signaling. An understanding of the ROS-mediated cytokine signaling crosstalk may explain the molecular basis of side effects of cytokine therapies in a variety of human diseases. It has been believed that the cytokine-activated JAK-STAT pathway operates directly from the cell surface to the nucleus via protein-protein and DNA-protein interactions, without involving any second messengers. This study reveals a role for ROS as a second messenger in the amplification of IL-4-mediated signal transduction in both *cis* and *trans*.

EXPERIMENTAL PROCEDURES

Cells and Reagents

A549, 293T, and NIH 3T3 cells were maintained in Dulbecco's modified Eagle's medium (DMEM) supplemented with 10% fetal calf serum (FCS). Immortalized MEFs from *Ptpn1*$^{+/+}$ and *Ptpn1*$^{-/-}$ mice were maintained in DMEM supplemented with 15% FCS (Buckley et al., 2002). Single-cell suspensions were prepared from mouse spleens and cultured in Iscove's modified Dulbecco's medium (IMDM) supplemented with 10% FCS. Cells obtained by flushing the mouse femur bone marrow were cultured in complete DMEM supplemented with 10% FCS and 20% L929-conditioned medium (as a source of M-CSF) for differentiating them into macrophages (Haque et al., 1998). For development of mast cells, the bone marrow-derived cells were cultured for 3–4 weeks in RPMI-1640 medium supplemented with 10% FCS, 10 mM HEPES, 1X MEM essential amino acids, 1 mM sodium pyruvate, 10 μM β-mercaptoethanol, and 20% WEHI-3 conditioned medium (as a source of IL-3), and cells were used when more than 95% of them stained positive with toluidine blue (Yuan et al., 1998).

All recombinant cytokines and anti-oxy-PTP were purchased from R&D Systems. Apocynin, DPI, AG490, LY294002, wortmannin, U0126, BAPTA-AM, U73122, Go6976, and calphostin C were obtained from Calbiochem. Nifedipine, heparin, and anti-FLAG-conjugated agarose beads were purchased from Sigma. All antibodies used for T cell isolation, differentiation, and analyses were from BD PharMingen. Anti-phospho (Tyrosine641)-STAT6 and anti-phospho-tyrosine PY100 were purchased from Cell Signaling Technology, and anti-V5 was from Invitrogen. Anti-STAT6, anti-β-actin, anti-FLAG, and anti-goat HRP were obtained from Santa Cruz, and anti-PTP1B was from BD Transduction. Anti-mouse HRP and anti-rabbit HRP were purchased from Amersham Biosciences.

All animal experiments were conducted according to the guidelines of our Institutional Animal Care and Use Committee.

Intracellular ROS Assays

ROS were measured fluorimetrically with CM-H_2DCFDA probe (Choi et al., 2005; Myhre et al., 2003). In brief, adherent cells were washed twice with Hank's balanced salt solution (HBSS), incubated with 5 μM CM-H_2DCFDA in HBSS for 10 min at 37°C in 5% CO_2, washed, and stimulated with indicated cytokine at 37°C under a Leica DMIRB inverted microscope (Leica Microsystems) equipped with a Retiga EXi Cooled CCD Camera (Q Imaging, Burnby) with a Ex_{490nm} and standard fluorescein filter. Images were taken every 10 s, and fluorescence signals were quantified with Image Pro Plus software (Media Cybernatics). Each value in relative fluorescence units (RFU) represents mean ± SEM of three independent measurements; each measurement represents the mean fluorescence signals of five equivalent fields (approximately same number of cells). For measuring ROS for longer time periods (>5 min), cells were loaded with CM-H_2DCFDA, trypsinized, and resuspended in HBSS, and changes in fluorescence signals were measured with flow cytometry (FACScan, Beckton-Dickinson). ROS produced by nonadherent cells were measured with Victor^2 Wallace Mutichannel Reader (Perkin Elmer) with Ex_{495nm} and Em_{535nm} filters.

Electrophoretic Mobility Shift, Super-Shift, and Luciferase Assays

EMSA was performed with 10 μg proteins of whole-cell extracts and 0.2 ng of ^{32}P-labeled high-affinity STAT6-specific probe (Haque et al., 2000). Cell extracts were incubated with 2 μg of normal rabbit IgG or STAT6 antibody prior to incubation with 0.2 ng of radiolabeled olionucleotide duplex for 20 min for super-shift assay or with 10 ng or 50 ng of unlabeled wild-type or mutant oligonucleotide duplex for competition assay. The sequences for the sense strand of the oligonucleotide are as follows: 5′-GATCGCTCTTCTTCCCAG*GAA*CTCA-ATG-3′ (wild-type) and 5′-GATCG-CTCTTCTTCCCAGGGGCTCA ATG-3′ (mutant), with the conserved N6-GAS sequence underlined (Haque et al., 2000) and the mutated nucleotides italicized. The DNA-protein complexes were resolved on native 6% polyacrylamide gels, dried, and visualized after incubation at −80°C. Luciferase assay was performed with the Dual Luciferase Assay Kit (Promega) according to the manufacturer's instructions.

Cloning, Site-Directed Mutagenesis, and Plasmid Constructs

Murine IL-4Rα cDNA was isolated from a NIH 3T3 cell-derived cDNA library by PCR and cloned in pcDNA3.1/V5-HisA (Invitrogen). For BRET assay, human

IL-4Rα was cloned in pRLuc-N3, and STAT6 and PTP1B (D181A) were cloned in pGFP^2-N2 (Perkin Elmer). The constructs for p22phox (wild-type and P156Q mutant), NOX1, NOXA1, NOXO1, NOX4, NOX5L, and p22phox shRNA (specific and scramble) are described (Kawahara et al., 2005). The wild-type (WT) and mutant (C174S) PTEN constructs were obtained from Charis Eng, and wild-type (WT) and mutant (T17N) RAC1 constructs were obtained from Olga Stenina. All point mutants were generated with Quick Change XL Site-Directed Mutagenesis Kit (Stratagene) according to the manufacturer's instructions.

DNA oligonucleotides encoding shRNA sequences with loop sequence (5′-TTCAAGAGA-3′) were cloned into pSuper-Neo (OligoEngine) according to the manufacturer's instructions. The specific target sense sequences were as follows: 5′-GAATTAGGCAAAGTGGGTT-3′ for NOX1, 5′-AAGAGCGA TTCTTTGCCCTAT-3′ for NOX5L, 5′-CGGGAAGACAAGTTCATGTACTT-3′ for PTEN, 5′-GAACAACCGGCTCTTCGT-3′ for PLCγ1, and 5′-AATCCTGACTTC CGAGAA-3′ for PLCγ2. The scramble versions of the target sequences were generated with siRNA Wizard (InVivogen) and cloned in pSuper-Neo vector (OligoEngine). All constructs were verified by nucleotide sequencing.

Transfection and Generation of Stable Clones

A549 and 293T cells were transfected with Lipofectamine 2000 (Invitrogen) and calcium phosphate coprecipitation, respectively (Haque et al., 2000), with transfection efficiencies of 70%–80% and ~90%, respectively. Stable clones of immortalized PTP1B-deficient MEFs were generated by selection with 150 μg/ml hygromycin B (Invitrogen) for 2 weeks.

Reverse Transcriptase-Polymerase Chain Reaction

For determination of mRNA levels, 1.0 μg of total RNA was used for first-strand cDNA synthesis according to the manufacturer's protocol (Invitrogen). One-tenth of cDNA was used as a template for 35 cycles of PCR with specific primer sets listed in Table S1.

RAC1 Activation Assay

A549 cells were treated with 20 μM LY294002 or DMSO (vehicle) for 2 hr, after which the cells were treated with IL-4 (20 ng/ml) for 5 min or left untreated. Cell lysates were used for detection of active RAC1 with the RAC1/Cdc42 Activation Assay Kit (Millipore) according to the manufacturer's instructions.

Measurement of Cytoplasmic Calcium Flux

For measurement of cytoplasmic calcium flux, cells were incubated with the calcium indicator dye Fluo4-AM (1 μM) for 30 min in complete DMEM according to the manufacturer's instructions (Molecular Probes). Before measurement of fluorescence signals, cells were washed twice with phenol red-free DMEM and incubated for another 15 min for complete hydrolysis of intracellular AM-esters. Images of cells were taken both before and after IL-4 stimulation, at every 2 s for 6 min at 37°C. Images were obtained with Leica SP-2 AOBS confocal microscope (Leica-Microsystems) with an HCX PL APO 40×/1.25 NA oil-immersion objective lens (Murata et al., 2004), with minor modifications. Fluo4 was excited with the 488 nm line of an argon laser, and its fluorescence emission was recorded between 500 and 550 nm with the built-in spectrophotomer. Illumination intensity was kept to a minimum (50 μW) for avoidance of phototoxicity, and the pinhole was set to 2 Airy units. Fluorescence signals were quantified with Leica confocal software (Leica-Microsystems).

In Vitro T Cell Differentiation

Single-cell suspensions of mouse lymph node cells were incubated with FITC-conjugated anti-CD8, anti-B220, anti-MHC class II (Fh2d), and anti-FcγR and then incubated with anti-FITC microbeads (Miltenyi Biotec). The negative fraction obtained after magnetic separation with an LS magnetic column (Miltenyi Biotec) contained >95% CD4$^+$ T cells. These cells were stained with PE-conjugated anti-CD44, and naive CD4$^+$ T cells were sorted with a FACSVantage SE cell sorter (Becton Dickinson). 1 × 10^6 purified naive CD4$^+$ T cells were cultured in 12-well plates in the presence of 3 μg/ml of anti-CD3 and 3 μg/ml of anti-CD28, with 5 × 10^6 T cell-depleted splenocytes. For Th1 cell differentiation, murine IL-12 (10 ng/ml) and anti-IL-4 (10 μg/ml) were added to the culture media. For Th2 cell differentiation, murine IL-4 (1000 U/ml) was added along with anti-IL-12 (10 μg/ml) and anti-IFN-γ (10 μg/ml). After 72 hr, the cells were harvested and restimulated with immobilized anti-CD3 (3 μg/ml) and anti-CD28 (3 μg/ml) for 6 hr in the presence of 2 μM monensin (Calbiochem) for the last 2 hr. The cells were fixed with 4% paraformaldehyde, permeabilized in buffer (PBS containing 0.1% BSA and 0.5% Triton X-100), and stained with FITC-conjugated anti-IFN-γ and PE-conjugated anti-IL-4. The expression of intracellular cytokines was determined with a FACSCalibur (Becton Dickinson) and analyzed with FlowJo software (Treestar).

Chemical Crosslinking, Immunoprecipitation, and Immunoblotting

Chemical crosslinking, immunoprecipitation, and immunoblotting of proteins were performed as described (Maiti et al., 2005).

BRET Assay

BRET assay was performed following the method of Pfleger and Eidne (Pfleger and Eidne, 2006). In brief, 293T cells were transfected with 1.0 μg of the donor plasmid pIL-4Rα-LUC-N3 and 3.0 μg of an acceptor plasmid pGFP^2-N2 (empty vector), STAT6-GFP^2-N2 or PTP1B-D181A-GFP^2-N2, with Lipofectamine 2000 (Invitrogen). After 48 hr, cells were washed with PBS and collected in BRET^2 buffer (Dulbecco's PBS supplemented with 0.05 g/l $CaCl_2$, 0.05 g/l $MgCl_2$, and 0.1 g/l glucose), washed twice, and resuspended at 2.5 × 10^7 cells/ml. Cell suspensions in 96-well plates (50 μl/well) were stimulated with 20 ng/ml of IL-4 or left untreated, followed by addition of DeepBlueC (Perkin Elmer). Fluorescence signals were measured at every 30 s with Victor^3 Wallace Multichannel Reader (Perkin Elmer) with Ex_{395nm} and Em_{510nm}. For each time point, BRET ratio was calculated as ($fluorescence_{510nm}$/luminescence) − ($fluorescence_{510nm}$ for donor only cells/luminescence). Each point represents mean ± SE (n = 3).

ROS-Induced Oxidation of PTP1B

PTP1B oxidation was measured as described (Persson et al., 2004), with minor modifications. For elimination of spontaneous PTP1B oxidation during cell lysis, buffers were extensively deoxygenated by bubbling nitrogen gas, and cell lysis was performed in an anaerobic chamber with a continuous flow of nitrogen gas. After indicated treatments, cells were washed with deoxygenated cold PBS and lysed with deoxygenated lysis buffer (20 mM Tris [pH 7.5], 1% NP-40, 10% glycerol, 1 mM benzamidine, and 1.4 μg/ml aprotenin) in the presence or absence of 100 mM iodoacetic acid (IAA). IAA alkylates all cysteines except the reversibly oxidized ones. Cell lysates were immunoprecipitaed with anti-PTP1B, immobilized on protein G sepharose beads, and incubated with 10 mM DTT to reduce the reversibly oxidized cysteine of PTP1B, which was subsequently oxidized irreversibly to cysteine-sulfonic acid by incubation with 100 μM PV for 1 hr at 4°C. The samples were then used for immunoblotting with a monoclonal antibody raised against a peptide corresponding to the conserved PTP active site ("Val-His-CysSO_3H-Ser-Ala-Gly") in which the catalytic cysteine (C215 in PTP1B) is irreversibly oxidized to cysteine-sulphonic acid.

Statistical and Densitometric Analyses

All experiments were performed at least three times. Statistical differences between different groups were determined with paired Student's t test. EMSA and immunoblot signals were quantified with ImageQuant (Molecular Dynamics).

SUPPLEMENTAL DATA

Supplemental Data include one table and thirteen figures and can be found with this article online at http://www.immunity.com/supplemental/S1074-7613(08)00429-9.

ACKNOWLEDGMENTS

We thank T.A. Hamilton, S. Datta, J. Dasgupta, C. Eng, O.I. Stenina, J. Kusari, A. Guha, and J.E. Dixon for sharing of reagents, J.A. Drazba for assistance in imaging, and T. Koeck and K.S. Aulak for technical assistance. We also thank J.A. Houghton, S.C. Erzurum, F.H. Hsieh, G.C. Sen, R.H. Silverman, and B. Raychaudhuri for comments. This work was supported by grants R01 GM060533 and R01 CA095006 from the National Institutes of Health to S.J.H.

Received: May 31, 2007
Revised: May 20, 2008
Accepted: July 23, 2008
Published: October 16, 2008

REFERENCES

Banfi, B., Molnar, G., Maturana, A., Steger, K., Hegedus, B., Demaurex, N., and Krause, K.H. (2001). A Ca(2+)-activated NADPH oxidase in testis, spleen, and lymph nodes. J. Biol. Chem. *276*, 37594–37601.

Banfi, B., Tirone, F., Durussel, I., Knisz, J., Moskwa, P., Molnar, G.Z., Krause, K.H., and Cox, J.A. (2004). Mechanism of Ca2+ activation of the NADPH oxidase 5 (NOX5). J. Biol. Chem. *279*, 18583–18591.

Buckley, D.A., Cheng, A., Kiely, P.A., Tremblay, M.L., and O'Connor, R. (2002). Regulation of insulin-like growth factor type I (IGF-I) receptor kinase activity by protein tyrosine phosphatase 1B (PTP-1B) and enhanced IGF-I-mediated suppression of apoptosis and motility in PTP-1B-deficient fibroblasts. Mol. Cell. Biol. *22*, 1998–2010.

Cheng, G., Diebold, B.A., Hughes, Y., and Lambeth, J.D. (2006). Nox1-dependent reactive oxygen generation is regulated by Rac1. J. Biol. Chem. *281*, 17718–17726.

Choi, M.H., Lee, I.K., Kim, G.W., Kim, B.U., Han, Y.H., Yu, D.Y., Park, H.S., Kim, K.Y., Lee, J.S., Choi, C., et al. (2005). Regulation of PDGF signalling and vascular remodelling by peroxiredoxin II. Nature *435*, 347–353.

Cool, R.H., Merten, E., Theiss, C., and Acker, H. (1998). Rac1, and not Rac2, is involved in the regulation of the intracellular hydrogen peroxide level in HepG2 cells. Biochem. J. *332*, 5–8.

Cross, A.R., and Jones, O.T. (1986). The effect of the inhibitor diphenylene iodonium on the superoxide-generating system of neutrophils. Specific labelling of a component polypeptide of the oxidase. Biochem. J. *237*, 111–116.

DeSilva, D.R., Jones, E.A., Favata, M.F., Jaffee, B.D., Magolda, R.L., Trzaskos, J.M., and Scherle, P.A. (1998). Inhibition of mitogen-activated protein kinase kinase blocks T cell proliferation but does not induce or prevent anergy. J. Immunol. *160*, 4175–4181.

Duran, A., Rodriguez, A., Martin, P., Serrano, M., Flores, J.M., Leitges, M., Diaz-Meco, M.T., and Moscat, J. (2004). Crosstalk between PKCzeta and the IL4/Stat6 pathway during T-cell-mediated hepatitis. EMBO J. *23*, 4595–4605.

Elchebly, M., Payette, P., Michaliszyn, E., Cromlish, W., Collins, S., Loy, A.L., Normandin, D., Cheng, A., Himms-Hagen, J., Chan, C.C., et al. (1999). Increased insulin sensitivity and obesity resistance in mice lacking the protein tyrosine phosphatase-1B gene. Science *283*, 1544–1548.

Fischer, E.H., Charbonneau, H., and Tonks, N.K. (1991). Protein tyrosine phosphatases: A diverse family of intracellular and transmembrane enzymes. Science *253*, 401–406.

Flint, A.J., Tiganis, T., Barford, D., and Tonks, N.K. (1997). Development of "substrate-trapping" mutants to identify physiological substrates of protein tyrosine phosphatases. Proc. Natl. Acad. Sci. USA *94*, 1680–1685.

Frey, R.S., Gao, X., Javaid, K., Siddiqui, S.S., Rahman, A., and Malik, A.B. (2006). Phosphatidylinositol 3-kinase gamma signaling through protein kinase Czeta induces NADPH oxidase-mediated oxidant generation and NF-kappaB activation in endothelial cells. J. Biol. Chem. *281*, 16128–16138.

Fu, X., Beer, D.G., Behar, J., Wands, J., Lambeth, D., and Cao, W. (2006). cAMP-response element-binding protein mediates acid-induced NADPH oxidase NOX5-S expression in Barrett esophageal adenocarcinoma cells. J. Biol. Chem. *281*, 20368–20382.

Fukuchi, K., Watanabe, H., Tomoyasu, S., Ichimura, S., Tatsumi, K., and Gomi, K. (2000). Phosphatidylinositol 3-kinase inhibitors, Wortmannin or LY294002, inhibited accumulation of p21 protein after gamma-irradiation by stabilization of the protein. Biochim. Biophys. Acta *1496*, 207–220.

Gschwendt, M., Dieterich, S., Rennecke, J., Kittstein, W., Mueller, H.J., and Johannes, F.J. (1996). Inhibition of protein kinase C mu by various inhibitors. Differentiation from protein kinase c isoenzymes. FEBS Lett. *392*, 77–80.

Haque, S.J., Harbor, P., Tabrizi, M., Yi, T., and Williams, B.R. (1998). Protein-tyrosine phosphatase Shp-1 is a negative regulator of IL-4- and IL-13-dependent signal transduction. J. Biol. Chem. *273*, 33893–33896.

Haque, S.J., Harbor, P.C., and Williams, B.R. (2000). Identification of critical residues required for suppressor of cytokine signaling-specific regulation of interleukin-4 signaling. J. Biol. Chem. *275*, 26500–26506.

Haque, S.J., and Sharma, P. (2006). Interleukins and STAT signaling. Vitam. Horm. *74*, 165–206.

Haque, S.J., Wu, Q., Kammer, W., Friedrich, K., Smith, J.M., Kerr, I.M., Stark, G.R., and Williams, B.R. (1997). Receptor-associated constitutive protein tyrosine phosphatase activity controls the kinase function of JAK1. Proc. Natl. Acad. Sci. USA *94*, 8563–8568.

Harkins, A.B., Kurebayashi, N., and Baylor, S.M. (1993). Resting myoplasmic free calcium in frog skeletal muscle fibers estimated with fluo-3. Biophys. J. *65*, 865–881.

Heldin, C.H. (1995). Dimerization of cell surface receptors in signal transduction. Cell *80*, 213–223.

Ho, J.L., Zhu, B., He, S., Du, B., and Rothman, R. (1994). Interleukin 4 receptor signaling in human monocytes and U937 cells involves the activation of a phosphatidylcholine-specific phospholipase C: A comparison with chemotactic peptide, FMLP, phospholipase D, and sphingomyelinase. J. Exp. Med. *180*, 1457–1469.

Ikizawa, K., Kajiwara, K., Koshio, T., and Yanagihara, Y. (1994). Possible role of tyrosine kinase activity in interleukin 4-induced expression of germ-line C epsilon transcripts in a human Burkitt lymphoma B-cell line, DND39. J. Allergy Clin. Immunol. *94*, 620–624.

Ikizawa, K., and Yanagihara, Y. (2000). Possible involvement of Shc in IL-4-induced germline epsilon transcription in a human B cell line. Biochem. Biophys. Res. Commun. *268*, 54–59.

Jagnandan, D., Church, J.E., Banfi, B., Stuehr, D.J., Marrero, M.B., and Fulton, D.J. (2007). Novel mechanism of activation of NADPH oxidase 5. calcium sensitization via phosphorylation. J. Biol. Chem. *282*, 6494–6507.

Jarvis, W.D., Turner, A.J., Povirk, L.F., Traylor, R.S., and Grant, S. (1994). Induction of apoptotic DNA fragmentation and cell death in HL-60 human promyelocytic leukemia cells by pharmacological inhibitors of protein kinase C. Cancer Res. *54*, 1707–1714.

Kawahara, T., Ritsick, D., Cheng, G., and Lambeth, J.D. (2005). Point mutations in the proline-rich region of p22phox are dominant inhibitors of Nox1- and Nox2-dependent reactive oxygen generation. J. Biol. Chem. *280*, 31859–31869.

Kubes, P., Suzuki, M., and Granger, D.N. (1991). Nitric oxide: An endogenous modulator of leukocyte adhesion. Proc. Natl. Acad. Sci. USA *88*, 4651–4655.

Lambeth, J.D. (2004). NOX enzymes and the biology of reactive oxygen. Nat. Rev. Immunol. *4*, 181–189.

Lambeth, J.D., Kawahara, T., and Diebold, B. (2007). Regulation of Nox and Duox enzymatic activity and expression. Free Radic. Biol. Med. *43*, 319–331.

Lee, S.R., Kwon, K.S., Kim, S.R., and Rhee, S.G. (1998). Reversible inactivation of protein-tyrosine phosphatase 1B in A431 cells stimulated with epidermal growth factor. J. Biol. Chem. *273*, 15366–15372.

Mahadev, K., Zilbering, A., Zhu, L., and Goldstein, B.J. (2001). Insulin-stimulated hydrogen peroxide reversibly inhibits protein-tyrosine phosphatase 1b in vivo and enhances the early insulin action cascade. J. Biol. Chem. *276*, 21938–21942.

Maiti, N.R., Sharma, P., Harbor, P.C., and Haque, S.J. (2005). Serine phosphorylation of Stat6 negatively controls its DNA-binding function. J. Interferon Cytokine Res. *25*, 553–563.

Meng, T.C., Fukada, T., and Tonks, N.K. (2002). Reversible oxidation and inactivation of protein tyrosine phosphatases in vivo. Mol. Cell *9*, 387–399.

Meydan, N., Grunberger, T., Dadi, H., Shahar, M., Arpaia, E., Lapidot, Z., Leeder, J.S., Freedman, M., Cohen, A., Gazit, A., et al. (1996). Inhibition of acute lymphoblastic leukaemia by a Jak-2 inhibitor. Nature *379*, 645–648.

Murata, T., Hori, M., Sakamoto, K., Karaki, H., and Ozaki, H. (2004). Dexamethasone blocks hypoxia-induced endothelial dysfunction in organ-cultured pulmonary arteries. Am. J. Respir. Crit. Care Med. *170*, 647–655.

Myers, M.P., Andersen, J.N., Cheng, A., Tremblay, M.L., Horvath, C.M., Parisien, J.P., Salmeen, A., Barford, D., and Tonks, N.K. (2001). TYK2 and JAK2 are substrates of protein-tyrosine phosphatase 1B. J. Biol. Chem. *276*, 47771–47774.

Myers, M.P., Stolarov, J.P., Eng, C., Li, J., Wang, S.I., Wigler, M.H., Parsons, R., and Tonks, N.K. (1997). P-TEN, the tumor suppressor from human chromosome 10q23, is a dual-specificity phosphatase. Proc. Natl. Acad. Sci. USA *94*, 9052–9057.

Myhre, O., Andersen, J.M., Aarnes, H., and Fonnum, F. (2003). Evaluation of the probes 2′,7′-dichlorofluorescin diacetate, luminol, and lucigenin as indicators of reactive species formation. Biochem. Pharmacol. *65*, 1575–1582.

Nelms, K., Keegan, A.D., Zamorano, J., Ryan, J.J., and Paul, W.E. (1999). The IL-4 receptor: Signaling mechanisms and biologic functions. Annu. Rev. Immunol. *17*, 701–738.

O'Shea, J.J., Gadina, M., and Schreiber, R.D. (2002). Cytokine signaling in 2002: New surprises in the Jak/Stat pathway. Cell *109* (*Suppl*), S121–S131.

Ohara, J., and Paul, W.E. (1987). Receptors for B-cell stimulatory factor-1 expressed on cells of haematopoietic lineage. Nature *325*, 537–540.

Park, H.S., Lee, S.H., Park, D., Lee, J.S., Ryu, S.H., Lee, W.J., Rhee, S.G., and Bae, Y.S. (2004). Sequential activation of phosphatidylinositol 3-kinase, beta Pix, Rac1, and Nox1 in growth factor-induced production of H2O2. Mol. Cell. Biol. *24*, 4384–4394.

Persson, C., Sjoblom, T., Groen, A., Kappert, K., Engstrom, U., Hellman, U., Heldin, C.H., den Hertog, J., and Ostman, A. (2004). Preferential oxidation of the second phosphatase domain of receptor-like PTP-alpha revealed by an antibody against oxidized protein tyrosine phosphatases. Proc. Natl. Acad. Sci. USA *101*, 1886–1891.

Pfleger, K.D., and Eidne, K.A. (2006). Illuminating insights into protein-protein interactions using bioluminescence resonance energy transfer (BRET). Nat. Methods *3*, 165–174.

Reid, K., Guo, T.Z., Davies, M.F., and Maze, M. (1997). Nifedipine, an L-type calcium channel blocker, restores the hypnotic response in rats made tolerant to the alpha-2 adrenergic agonist dexmedetomidine. J. Pharmacol. Exp. Ther. *283*, 993–999.

Rhee, S.G., Bae, Y.S., Lee, S.R., and Kwon, J. (2000). Hydrogen peroxide: A key messenger that modulates protein phosphorylation through cysteine oxidation. Sci. STKE *2000*, PE1.

Salmeen, A., Andersen, J.N., Myers, M.P., Meng, T.C., Hinks, J.A., Tonks, N.K., and Barford, D. (2003). Redox regulation of protein tyrosine phosphatase 1B involves a sulphenyl-amide intermediate. Nature *423*, 769–773.

Seuwen, K., and Boddeke, H.G. (1995). Heparin-insensitive calcium release from intracellular stores triggered by the recombinant human parathyroid hormone receptor. Br. J. Pharmacol. *114*, 1613–1620.

Stam, J.C., Michiels, F., van der Kammen, R.A., Moolenaar, W.H., and Collard, J.G. (1998). Invasion of T-lymphoma cells: Cooperation between Rho family GTPases and lysophospholipid receptor signaling. EMBO J. *17*, 4066–4074.

Tsien, R.Y. (1980). New calcium indicators and buffers with high selectivity against magnesium and protons: Design, synthesis, and properties of prototype structures. Biochemistry *19*, 2396–2404.

van Montfort, R.L., Congreve, M., Tisi, D., Carr, R., and Jhoti, H. (2003). Oxidation state of the active-site cysteine in protein tyrosine phosphatase 1B. Nature *423*, 773–777.

Wery-Zennaro, S., Zugaza, J.L., Letourneur, M., Bertoglio, J., and Pierre, J. (2000). IL-4 regulation of IL-6 production involves Rac/Cdc42- and p38 MAPK-dependent pathways in keratinocytes. Oncogene *19*, 1596–1604.

Yamada, T., Zhu, D., Saxon, A., and Zhang, K. (2002). CD45 controls interleukin-4-mediated IgE class switch recombination in human B cells through its function as a Janus kinase phosphatase. J. Biol. Chem. *277*, 28830–28835.

Yuan, Q., Gurish, M.F., Friend, D.S., Austen, K.F., and Boyce, J.A. (1998). Generation of a novel stem cell factor-dependent mast cell progenitor. J. Immunol. *161*, 5143–5146.

Zamorano, J., Rivas, M.D., Garcia-Trinidad, A., Qu, C.K., and Keegan, A.D. (2003). Phosphatidylcholine-specific phospholipase C activity is necessary for the activation of STAT6. J. Immunol. *171*, 4203–4209.